Optical properties of biological tissues: a review

2013 Phys. Med. Biol. 58 R37

(http://iopscience.iop.org/0031-9155/58/11/R37)

Phys. Med. Biol. **58** (2013) R37–R61 doi:10.1088/0031-9155/58/11/R37

TOPICAL REVIEW

Optical properties of biological tissues: a review

Steven L Jacques[1,2]

[1] Department of Biomedical Engineering, Oregon Health Science University, 3303 SW Bond Ave, Portland, OR 97239, USA
[2] Department of Dermatology, Oregon Health Science University, 3303 SW Bond Ave, Portland, OR 97239, USA

E-mail: jacquess@ohsu.edu

Received 11 January 2013, in final form 26 February 2013
Published 10 May 2013
Online at stacks.iop.org/PMB/58/R37

Abstract
A review of reported tissue optical properties summarizes the wavelength-dependent behavior of scattering and absorption. Formulae are presented for generating the optical properties of a generic tissue with variable amounts of absorbing chromophores (blood, water, melanin, fat, yellow pigments) and a variable balance between small-scale scatterers and large-scale scatterers in the ultrastructures of cells and tissues.

(Some figures may appear in colour only in the online journal)

Introduction

The optical properties of a tissue affect both diagnostic and therapeutic applications of light. The ability of light to penetrate a tissue, interrogate the tissue components, then escape the tissue for detection is key to diagnostic applications. The ability of light to penetrate a tissue and deposit energy via the optical absorption properties of the tissue is key to therapeutic applications. Hence, specifying the optical properties of a tissue is the first step toward properly designing devices, interpreting diagnostic measurements or planning therapeutic protocols. The second step is to use the optical properties in a light transport model to predict the light distribution and energy deposition. This review will resist the temptation to describe light transport, and will focus on the expected optical properties of various tissue types, and how to routinely formulate the optical properties of a tissue at any given wavelength.

In the past, reviews have tabulated the optical properties (absorption, scattering, anisotropy, reduced scattering, refractive index) of various tissues measured at some (or many) wavelengths and such tabulations have been useful (Cheong 1995, Kim and Wilson 2011, Sandell and Zhu 2011, Bashkatov *et al* 2011). But if one needed to know the optical properties of a particular tissue *in vivo*, would one be confident in using a tabulated value? Firstly, the tabulated values may not be accurate due to measurement artifacts. Secondly, the living tissue of a particular person is subject to variations in blood content, water content, collagen content and fiber development. The variations are significant from person to person,

site to site on one person or even time to time on one site. The tabulated values may not include the wavelength of interest. Perhaps it is more useful to understand the expected standard behavior of optical properties, and to anticipate the variation in tissue constitution that yields the tissue optical properties at any desired wavelength.

This review summarizes the tissue optical absorption coefficient, μ_a, in terms of the average hemoglobin (HGb) concentration (C_{HGb}) in the tissue or alternatively as whole blood volume fraction (B), the arterio-venous oxygen saturation (S) of HGb in the blood, the average water content (W) and the average fat content (F). These parameters scale standard absorption spectra. If there are other minor absorbers in the tissue (melanin, bilirubin, betacarotene, etc), they can be added to the tissue absorption.

The review summarizes the optical reduced scattering coefficient, μ_s', by the parameters (a, b), or alternatively (a', f_{Rayleigh}, b_{Mie}) (explained later). These parameters specify standard scattering behavior versus wavelength. Hence, data on at least three wavelengths is sufficient to allow prediction of scattering at all wavelengths in the UV, visible, near-IR range. The μ_s' and μ_a properties describe diffusion of light in a tissue and reflection of multiply scattered light from a tissue. These optical properties govern the reflectance from a tissue seen by a camera or the lateral diffusion of light within a tissue collected by an optical fiber probe.

The review also reviews reports of the tissue scattering coefficient, μ_s, and the angular function of single scattering, $p(\theta)$, that in turn allows calculation of the anisotropy, g, that characterizes the effectiveness of scattering. The real refractive index (n') of tissues is discussed, which pertains to interferometric measurements and some microscopy applications. These three parameters (μ_s, g, n') influence how light penetrates to a focus and returns to a microscope.

Section 1 offers an introduction to the basics of tissue optical properties. Section 2 considers the reduced scattering coefficient of tissues. Section 3 discusses the scattering coefficient and the anisotropy of scattering. Section 4 describes the refractive index. Section 5 summarizes the absorption properties of blood, water, melanin, fat and yellow pigments. Section 6 presents a bookkeeping scheme for predicting the optical properties at any wavelength based on the components of the tissue.

1. Introduction to tissue optical properties

The optical properties of a tissue are described in terms of the absorption coefficient, μ_a (cm^{-1}), the scattering coefficient μ_s (cm^{-1}), the scattering function $p(\theta,\psi)$ (sr^{-1}) where θ is the deflection angle of scatter and ψ is the azimuthal angle of scatter, and the real refractive index of the tissue, n'. An introduction to these properties is presented elsewhere (Cheong 1995, Jacques and Pogue 2008, Welch and van Gemert 2011).

The $p(\theta,\psi)$ is appropriate when discussing only a single or few scattering events, such as during transmission microscopy of thin tissue sections or during confocal reflectance microscopy, which includes optical coherence tomography. In thicker tissues where multiple scattering occurs and the orientations of scattering structures in the tissue are randomly oriented, the ψ dependence of scattering is averaged and hence ignored, and the multiple scattering averages the θ such that an average parameter, $g = \langle \cos\theta \rangle$, called the anisotropy of scatter, characterizes tissue scattering in terms of the relative forward versus backward direction of scatter. Figure 1 summarizes these properties and their inter-relationships.

Optical scattering can be described either as scattering by particles that have a refractive index different from the surrounding medium, or as scattering by a medium with a continuous but fluctuating refractive index. The particle description can be approximated by Mie theory, which describes the scattering from ideal spheres within a medium (Prahl and Jacques

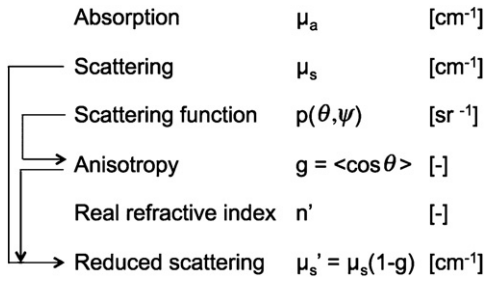

Figure 1. The optical properties of tissues.

2012). A mixture of spheres of different sizes can mimic the optical scattering behavior of a tissue. Continuum scattering theory describes tissue scattering in terms of the autocorrelation function for the spatial distribution of the fluctuating refractive index in a tissue (Schmitt and Kumar 1996, Xu and Alfano 2005, Rogers *et al* 2009, Yi and Backman 2012). The Wiener–Khinchin theorem relates an autocorrelation function to its corresponding power spectrum, and continuum scattering theory relates the spatial autocorrelation of refractive index fluctuations to the wavelength dependence of scatter. Both descriptions are adjusted to match experimental data and hence both are descriptors for the scattering behavior of tissues.

The terms *Rayleigh scattering* and *Mie scattering* are commonly used in the field of biomedical optics, with Rayleigh scattering referring to scattering by small particles or mass density fluctuations much smaller than the wavelength of light, and Mie scattering referring to scattering by particles comparable to or larger than the wavelength of light. But this common use of these terms is not actually correct. Mie scattering is the generic name for scattering by a sphere of any size, both small and large, and the common term Rayleigh scattering refers to the Rayleigh limit of Mie scattering due to particles much smaller than the wavelength of light. Nevertheless, the common usage of Rayleigh and Mie is followed in this review because it is familiar to many in our field.

2. The reduced scattering coefficient of tissues

A review of tissue μ_s' properties as a function of wavelength is presented, which is not exhaustive but sufficient to characterize the behavior of seven groups of tissues: skin, brain, breast, bone, other soft tissues, other fibrous tissues and fatty tissues. The data of $\mu_s'(\lambda)$ were fit with two equations:

$$\mu_s' = a\left(\frac{\lambda}{500\ (\text{nm})}\right)^{-b} \tag{1}$$

and alternatively

$$\mu_s'(\lambda) = a'\left(f_{\text{Ray}}\left(\frac{\lambda}{500\ (\text{nm})}\right)^{-4} + (1 - f_{\text{Ray}})\left(\frac{\lambda}{500\ (\text{nm})}\right)^{-b_{\text{Mie}}}\right). \tag{2}$$

In equation (1), the wavelength λ is normalized by a reference wavelength, 500 nm, to yield a dimensionless value, which is then raised to a power b, called the 'scattering power'. This term characterizes the wavelength dependence of μ_s'. The factor a is the value $\mu_s'(\lambda = 500\ \text{nm})$, which scales the wavelength-dependent term.

In equation (2), the wavelength dependence of scattering is described in terms of the separate contributions of Rayleigh and Mie scattering at the reference wavelength. The scaling factor a' equals $\mu_s'(\lambda = 500\ \text{nm})$. The Rayleigh scattering is $a' f_{\text{Ray}}(\lambda/500\ \text{nm})^{-4}$, and the

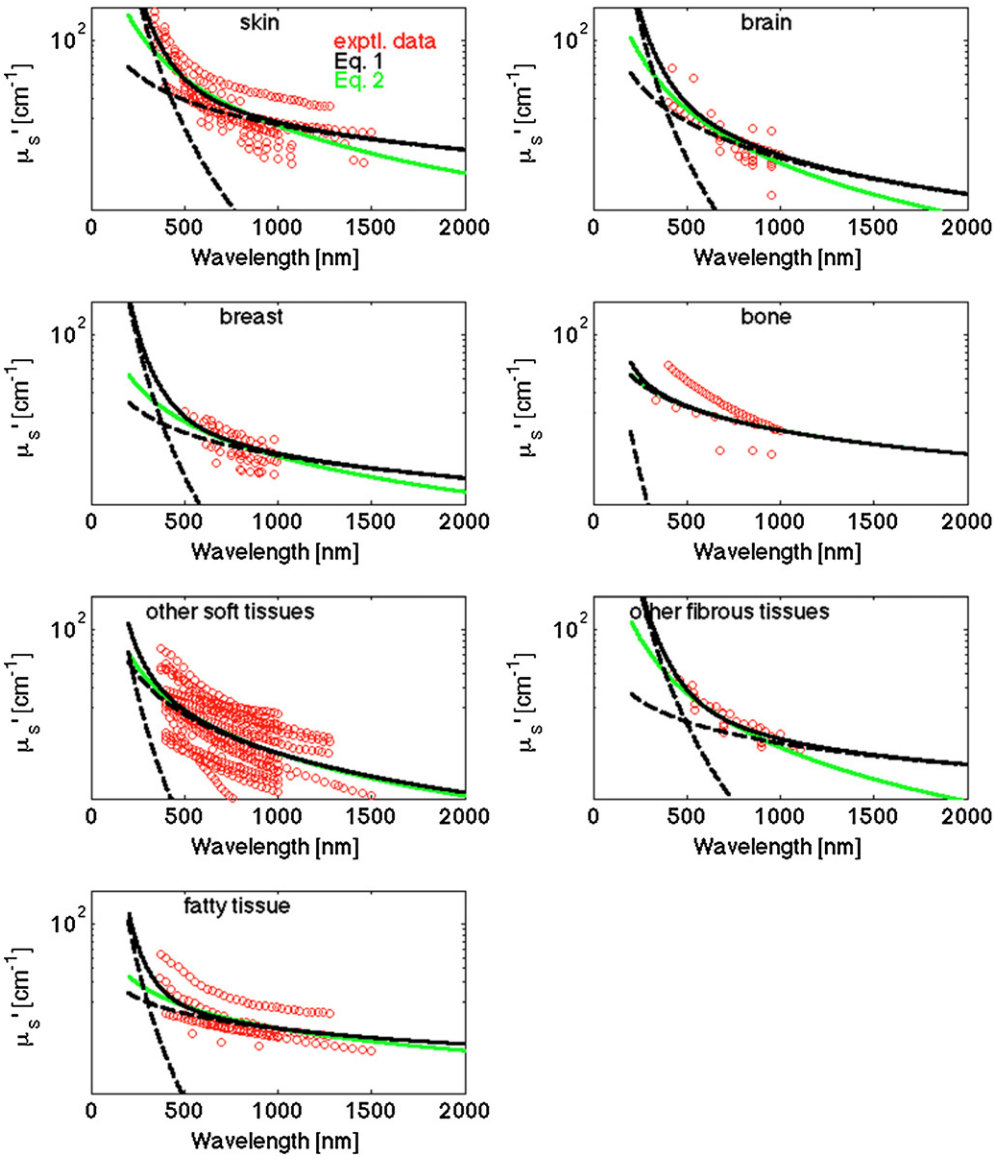

Figure 2. Reduced scattering coefficient spectra from the literature for the seven groups of tissues (red circles = data). The green line is the fit using equation (1). The black solid line is the fit using equation (2), with the black dashed lines showing the Rayleigh and Mie components of the fit.

Mie scattering is $a'(1 - f_{\mathrm{Ray}})(\lambda/500\ \mathrm{nm})^{-b_{\mathrm{Mie}}}$, where $1 - f_{\mathrm{Ray}}$ indicates the fraction of Mie scattering.

Table 1 summarizes the parameters of equations (1) and (2) obtained by analysis of the literature data for $\mu_s'(\lambda)$. Figure 2 displays the data for each of the seven tissue types. Also shown are the fits to the data using the mean parameters for equations (1) and (2) listed in table 1 for each data set.

Table 2 summarizes the mean values of the parameters for equations (1) and (2) as applied to each of the seven tissue types in table 1.

Table 1. Parameters specifying thereduced scattering coefficient of tissues: $a = \mu'_{s\,500\,\mathrm{nm}}$, such that $\mu'_s(\lambda) = a(\lambda/500\ \mathrm{nm})^{-b}$, equation (1); $aa = \mu'_{s\,500\,\mathrm{nm}}$, such that $\mu'_s(\lambda) = aa(f_{\mathrm{Ray}}(\lambda/500\ \mathrm{nm})^{-b} + f_{\mathrm{Mie}}(\lambda/500\ \mathrm{nm})^{-b_{\mathrm{Mie}}})$, equation (2); and $f_{\mathrm{Mie}} = 1 - f_{\mathrm{Ray}}$. (na = not available.)

#	a (cm^{-1})	b	a' (cm^{-1})	f_{Ray}	b_{Mie}	Ref.	Tissue
Skin							
1	48.9	1.548	45.6	0.22	1.184	Skin	Anderson *et al* 1982
2	47.8	2.453	42.9	0.76	0.351	Skin	Jacques 1996
3	37.2	1.390	42.6	0.40	0.919	Skin	Simpson *et al* 1998
4	60.1	1.722	58.3	0.31	0.991	Skin	Saidi *et al* 1995
5	29.7	0.705	36.4	0.48	0.220	Skin	Bashkatov *et al* 2011
6	45.3	1.292	43.6	0.41	0.562	Dermis	Salomatina *et al* 2006
7	68.7	1.161	66.7	0.29	0.689	Epidermis	Salomatina *et al* 2006
8	30.6	1.100	na	na	na	Skin	Alexandrakis *et al* 2005
Brain							
9	40.8	3.089	40.8	0.00	3.088	Brain	Sandell and Zhu 2011
10	10.9	0.334	13.3	0.36	0.000	Cortex (frontal lobe)	Bevilacqua *et al* 2000
11	11.6	0.601	15.7	0.53	0.000	Cortex (temporal lobe)	Bevilacqua *et al* 2000
12	20.0	1.629	29.1	0.81	0.000	Astrocytoma of optic nerve	Bevilacqua *et al* 2000
13	25.9	1.156	25.9	0.00	1.156	Normal optic nerve	Bevilacqua *et al* 2000
14	21.5	1.629	31.0	0.82	0.000	Cerebellar white matter	Bevilacqua *et al* 2000
15	41.8	3.254	41.8	0.00	3.254	Medulloblastoma	Bevilacqua *et al* 2000
16	21.4	1.200	21.4	0.00	1.200	Brain	Yi and Backman 2012
Breast							
17	31.8	2.741	31.8	0.00	2.741	Breast	Sandell and Zhu 2011
18	11.5	0.775	15.2	0.58	0.000	Breast	Sandell and Zhu 2011
19	24.8	1.544	24.8	0.00	1.544	Breast	Sandell and Zhu 2011
20	20.1	1.054	20.2	0.18	0.638	Breast	Sandell and Zhu 2011
21	14.6	0.410	18.1	0.41	0.000	Breast	Spinelli *et al* 2004
22	12.5	0.837	17.4	0.60	0.076	Breast, premenopausal	Cerussi *et al* 2001
23	8.3	0.617	11.2	0.54	0.009	Breast, postmenopausal	Cerussi *et al* 2001
24	10.5	0.464	10.5	0.00	0.473	Breast	Durduran *et al* 2002
Bone							
25	9.5	0.141	9.7	0.04	0.116	Skull	Bevilacqua *et al* 2000
26	20.9	0.537	20.9	0.00	0.537	Skull	Firbank *et al* 1993
27	38.4	1.470	na	na	na	Bone	Alexandrakis *et al* 2005
Other soft tissues							
28	9.0	0.617	11.5	0.61	0.000	Liver	Parsa *et al* 1989
29	13.0	0.926	13.0	0.00	0.926	Muscle	Tromberg 1996
30	12.2	1.448	13.0	0.44	0.731	Fibroadenoma breast	Peters *et al* 1990
31	18.8	1.620	18.8	0.00	1.620	Mucous tissue	Bashkatov *et al* 2011
32	28.1	1.507	27.7	0.23	1.165	SCC	Salomatina *et al* 2006
33	42.8	1.563	42.5	0.10	1.433	Infiltrative BCC	Salomatina *et al* 2006
34	31.9	1.371	31.5	0.15	1.157	Nodular BCC	Salomatina *et al* 2006
35	16.5	1.240	na	na	na	Bowel	Alexandrakis *et al* 2005
36	14.6	1.430	na	na	na	Heart wall	Alexandrakis *et al* 2005
37	35.1	1.510	na	na	na	Kidneys	Alexandrakis *et al* 2005
38	9.2	1.050	na	na	na	Liver&spleen	Alexandrakis *et al* 2005
39	25.4	0.530	na	na	na	Lung	Alexandrakis *et al* 2005
40	9.8	2.820	na	na	na	Muscle	Alexandrakis *et al* 2005
41	19.1	0.970	na	na	na	Stomach wall	Alexandrakis *et al* 2005
42	22.0	0.660	na	na	na	Whole blood	Alexandrakis *et al* 2005
43	16.5	1.640	16.5	0.00	1.640	Liver	Yi and Backman 2012
44	8.1	0.980	8.1	0.00	0.980	Lung	Yi and Backman 2012
45	8.3	1.260	8.3	0.00	1.260	Heart	Yi and Backman 2012

Table 1. (Continued.)

#	a (cm^{-1})	b	a' (cm^{-1})	f_{Ray}	b_{Mie}	Ref.	Tissue
Other fibrous tissues							
46	33.6	1.712	37.3	0.72	0.000	Tumor	Sandell and Zhu 2011
47	30.1	1.549	30.1	0.02	1.521	Prostate	Newman and Jacques 1991
48	27.2	1.768	29.7	0.61	0.585	Glandular breast	Peters *et al* 1990
49	24.1	1.618	25.8	0.49	0.784	Fibrocystic breast	Peters *et al* 1990
50	20.7	1.487	22.8	0.60	0.327	Carcinoma breast	Peters *et al* 1990
Fatty tissue							
51	13.7	0.385	14.7	0.16	0.250	Subcutaneous fat	Simpson *et al* 1998
52	10.6	0.520	11.2	0.29	0.089	Adipose breast	Peters *et al* 1990
53	15.4	0.680	15.4	0.00	0.680	Subcutaneous adipose	Bashkatov *et al* 2011
54	35.2	0.988	34.2	0.26	0.567	Subcut. fat	Salomatina *et al* 2006
55	21.6	0.930	21.1	0.17	0.651	Subcut. adipocytes	Salomatina *et al* 2006
56	14.1	0.530	na	na	na	Adipose	Alexandrakis *et al* 2005

Table 2. Average parameters for reduced scattering coefficient, μ_s', for tissues.

	a (cm^{-1})	b	a' (cm^{-1})	f_{Ray}	b_{Mie}
Skin					
Mean	46.0	1.421	48.0	0.409	0.702
SD	13.7	0.517	10.6	0.178	0.351
n	8	8	7	7	7
Brain					
Mean	24.2	1.611	27.4	0.315	1.087
SD	11.7	1.063	10.5	0.368	1.386
n	8	8	8	8	8
Breast					
Mean	16.8	1.055	18.7	0.288	0.685
SD	8.1	0.771	7.0	0.273	0.984
n	8	8	8	8	8
Bone					
Mean	22.9	0.716	15.3	0.022	0.326
SD	14.6	0.682	7.9	0.032	0.298
n	3	3	2	2	2
Other soft tissues					
Mean	18.9	1.286	19.1	0.153	1.091
SD	10.2	0.521	11.3	0.216	0.483
n	18	18	10	10	10
Other fibrous tissues					
Mean	27.1	1.627	29.2	0.489	0.644
SD	5.0	0.115	5.4	0.274	0.572
n	5	5	5	5	5
Fatty tissue					
Mean	18.4	0.672	19.3	0.174	0.447
SD	9.0	0.242	9.1	0.111	0.263
n	6	6	5	5	5

So which is better, equation (1) or equation (2)? The equations are equally good for routine prediction of tissue scattering for use in predicting behavior of light diffusion within the 400–1300 nm wavelength range. But outside this range in either the ultraviolet or the longer infrared, the two equations diverge. More data is needed, especially at longer wavelengths, to resolve which equation is better.

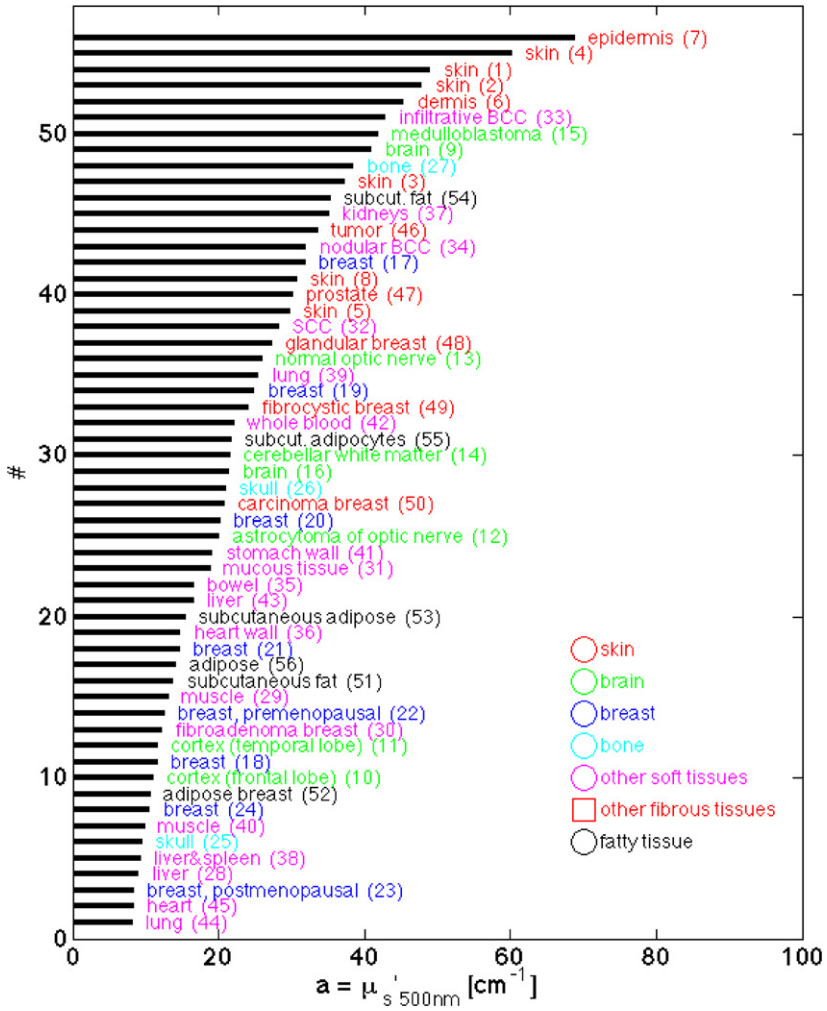

Figure 3. Ranking the tissues by their scattering at 500 nm, $\mu'_{s\,500\,\mathrm{nm}}$, specified by the parameter a in equation (1). The numbers in parentheses indicate the # in table 1.

The bigger issue is the variability of the a and a' values, which scale the wavelength-dependent terms in equations (1) and (2). In particular, the category 'other soft tissues' show significant variability in a and a'. Figure 3 ranks the data according to the value of a in equation (1), showing that skin and other fibrous tissues have higher values of a ($\mu'_{s\,500\,\mathrm{nm}}$) than other tissues. Breast tissues are seen at both low and high scattering, perhaps dependent on the relative fibrous versus fatty character of the particular breast.

If one is interested in using the scattering properties to characterize the sub-μm structure of a cell, then the details of equations (1) and (2) become important. In general, cellular tissues will present a simple λ^{-b} behavior, and equation (1) is sufficient. Cellular tissues with a high density of mitochondria (Beauvoit *et al* 1995) or lysosomes (Wilson *et al* 2007) will present Rayleigh scattering due to the high density of lipid membranes, which causes an elevation of b in equation (1) and an elevation of f_{Ray} in equation (2). Collagenous tissues, such as skin and some fibrous tissues, present much more Rayleigh scattering putatively due to the 70 nm

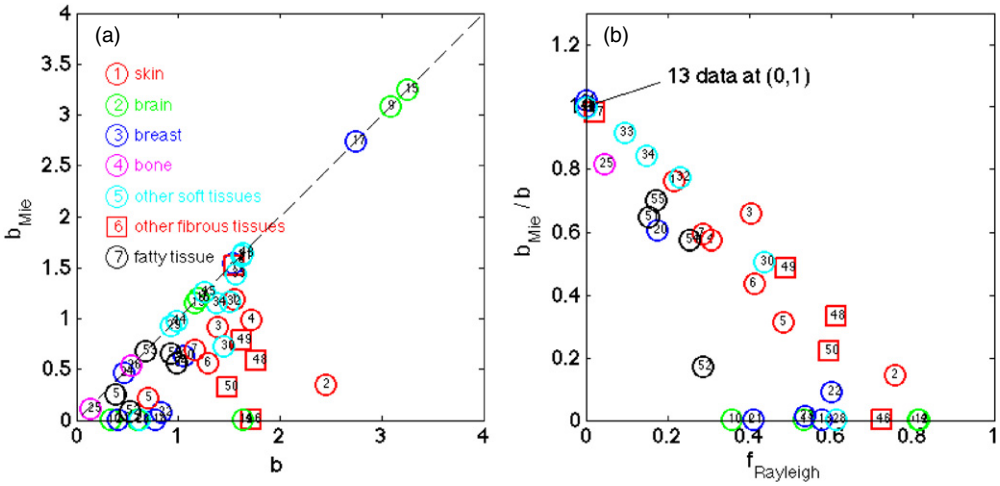

Figure 4. (a) Plot of b_{Mie} versus b in equations (2) and (1), respectively. (b) Plot of b_{Mie}/b versus f_{Rayleigh}. The data are from table 1. When f_{Rayleigh} is significant, b_{Mie} is less than b.

periodic density along collagen fibrils and the sub-100 nm inter-fibril spacings (Saidi *et al* 1995, Jacques 1996), which also elevates b and f_{Ray}.

Figure 4(a) plots b_{Mie} versus b, and shows some tissues tracking as $b_{\text{Mie}} = b$, while other tissues, especially the skin and fibrous tissues, show a lower b_{Mie} than b. When the data allow specification of both a short wavelength rise and a long wavelength stability in μ_s', then f_{Ray} can account for the Rayleigh scattering and b_{Mie} can account for the slower fall in μ_s' versus longer wavelengths. Figure 4(b) shows the ratio b_{Mie}/b versus f_{Ray}, illustrating the drop in b_{Mie} relative to b as f_{Ray} grows.

More data, especially at longer wavelengths, is needed to clarify if Mie scattering is indeed relatively wavelength independent ($b_{\text{Mie}} \leqslant 1$). If so, then equation (2) is a better descriptor than equation (1), and the short wavelength rise in μ_s' specifies an f_{Ray} that becomes a useful parameter for quantifying the scattering due to organelles and collagen fibrils. If not, then the entire spectrum is consistent with equation (1) and the simple $a(\lambda/\lambda_{\text{reference}})^{-b}$ behavior implies the corresponding autocorrelation of refractive index fluctuations (i.e. mass fluctuations) follows a simple form. Whether one form or the other is more useful remains to be seen. This question is an area of study that hopes to use changes in the structure of cells and tissues in the ∼50–600 nm range as a contrast parameter while imaging cells or tissues macroscopically. Such surveillance may prove useful in imaging the margins of cancers, for example.

3. Scattering μ_s and anisotropy g

The measurement of μ_s can be a difficult task. The measurement of μ_s is usually made by a collimated transmission measurement (T_c) through tissue of thickness L to specify $\mu_s = -\ln(T_c)/L$. But such measurements must be made through a thin tissue sample, on the scale of one mean free path (mfp $= 1/\mu_s$), which is typically 100 μm or less, or else multiple scattering becomes an issue. But preparing such thin tissues is not easy, and they are subject to desiccation. Also, the heterogeneity of tissues becomes apparent in such thin samples. Another issue is the solid angle of collection at the detector, which if too large will collect photons despite their being slightly deflected, thereby underestimating μ_s.

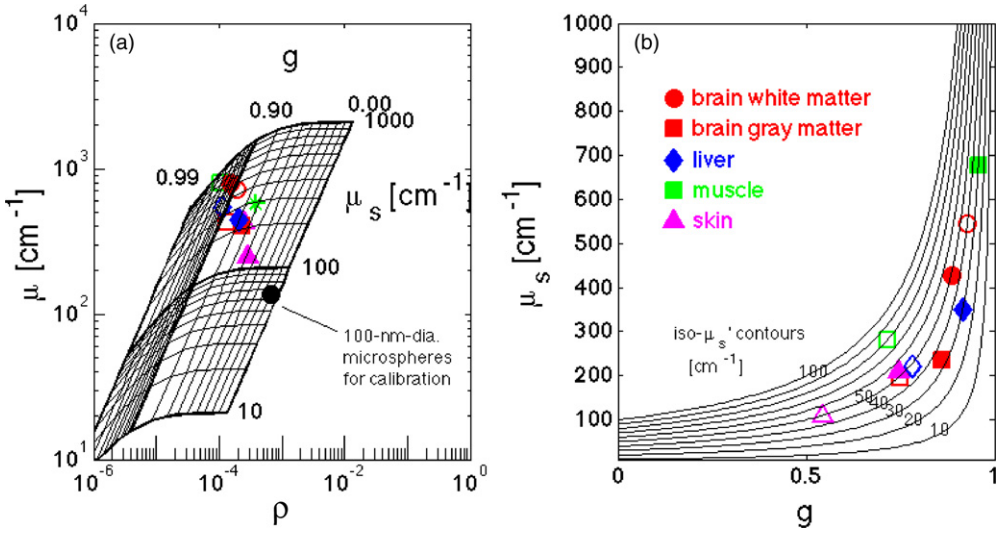

Figure 5. Scattering coefficient μ_s versus anisotropy g at 488 nm wavelength. (a) Experimental confocal reflectance data of attenuation (μ (cm^{-1})) versus depth of focus and absolute value of reflected signal (ρ, a mirror defines $\rho = 1$) (Samatham 2012). Grid shows the expected values of μ, ρ for various μ_s, g values. Open symbols are tissues exposed to saline. Closed symbols are tissues not directly contacted by saline, but kept moist via vapor pressure. (b) Plot of μ_s versus g using values specified in figure 4(a). Several iso-μ_s' contours are drawn, with tissues mostly in the range of 30–50 cm^{-1}.

Similarly, the measurement of g can be difficult. Direct measurement of $p(\theta)$ using goniometry involves measurement of the angular scattering of light by a thin tissue sample, which then allows calculation of g (see below). The concerns about local heterogeneity in a thin sample pertain to goniometry. Also, the measurements in the backward direction are often low, and must be well above any noise floor of measurement since the backward signal is critical to the net value of g. When measuring a thin tissue slab, the angle and intensity of exit from the tissue can be modified by refraction at the tissue/air or tissue/glass/air interface. Using a hemispherical lens coupled to the tissue allows exiting photons to encounter a glass/air interface perpendicularly, which mitigates refraction. Measurements of scattering around $\theta = 90$ can be experimentally complicated.

One approach toward measuring g is to use the values of μ_s' from diffuse light measurements and μ_s from collimated transmission measurements to deduce g: $g = 1 - \mu_s'/\mu_s$. While the μ_s' value is usually robust, the μ_s value may not be so reliable, as discussed above. An artifactual decrease in μ_s causes an artifactual decrease in g.

A recent approach (Gareau 2006, Samatham *et al* 2008, Jacques *et al* 2008) has been to measure the attenuation of backscattered reflectance collected by a confocal microscope as the focus is scanned down into a tissue. A high g value allows light to penetrate to the focus despite multiple scattering, and to return from the focus and still reach the pinhole of collection. However, a high g value reduces the amount of light backscattered at the focus which decreases the collected reflectance. The measurement of reflectance, $R(z_f) = \rho \exp(-\mu z_f)$, depends on two parameters, (1) the attenuation (μ (cm^{-1})) versus depth of focus and (2) the absolute value of reflected signal within the focus (ρ, a mirror defines $\rho = 1$). Together, μ and ρ specify the two unknown values μ_s and g.

Figure 5(a) shows the measurements at 488 nm wavelength of Samatham (2012) on freshly excised mouse tissues, illustrating how μ and ρ specify μ_s and g. Figure 5(b) plots μ_s

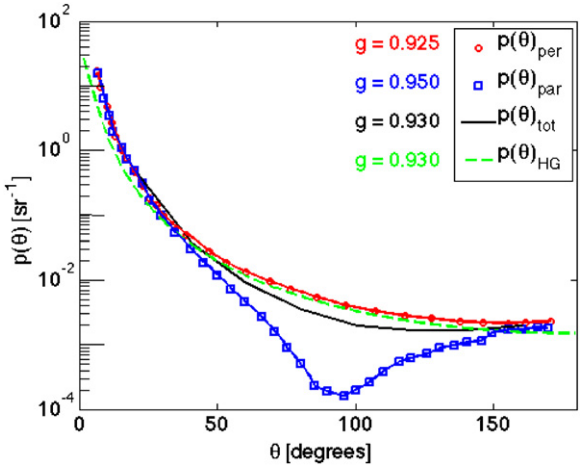

Figure 6. Angular scattering function, $p(\theta)$ (sr^{-1}), of cells in suspension (androgen-independent malignant rat prostate carcinoma cells). The data are taken from Mourant *et al* (2002), and plotted after normalizing so that equation (6) holds for $p(\theta)_{tot} = 0.5(p(\theta)_{per} + p(\theta)_{par})$. The $p(\theta)_{per}$ and $p(\theta)_{par}$ are the scattering for polarized light oriented perpendicular and parallel to the scattering plane (see text). The anisotropies of scattering, g, are indicated for each curve. The green line is the Henyey–Greenstein function for $g = 0.930$, which is the g value for the total scattering, showing an approximation to the cellular scattering.

versus g as well as iso-μ_s' contours. The data show that μ_s and g increase coordinately, while $\mu_s(1 - g)$ remains somewhat constant in the range of 30–50 cm^{-1}.

Mourant *et al* (2002) reported on the scattering properties of cultured cells in suspension. Figure 6 shows the scattering function $p(\theta)$ (sr^{-1}) for light polarized perpendicular to the scattering plane ($p(\theta)_{per}$) and for light polarized parallel to the scattering plane ($p(\theta)_{par}$). The scattering plane is defined as the plane containing the laser source, cell sample and the detector. The forward scattering is denoted by $\theta = 0^\circ$, and direct backscatter is denoted by $\theta = 180^\circ$. The cells show a very forward-directed scatter, with anisotropies of $g = 0.925$, 0.950 and 0.930 for the perpendicular, parallel and total scattering functions ($\arccos(0.925) = 22.3^\circ$, $\arccos(0.950) = 18.2^\circ$ and $\arccos(0.930) = 21.6^\circ$).

Xu *et al* (2008) reported on the angular and wavelength dependence of the scattering function $p(\theta, \lambda)$. Figure 7 shows the $p(\theta)$ for their cells (SiHa cells in phosphate buffered saline suspensions) at 633 nm wavelength. Their report is especially interesting because they demonstrated that the first 10° of angular deflection are dominated by the cell as a whole and by the nucleus, consistent with Mie scattering from large spheres. At wider angles >10°, the scattering was due to the small-scale refractive index fluctuations of the organelles, aggregates and membranes of the cell, and this broad scattering was modeled by a continuum model.

Jacques *et al* (1987) and Hall *et al* (2012) studied the goniometry of light transmission through tissues of varying sample thickness. The scattered light could be described by an equivalent Henyey–Greenstein function with an apparent g. As the tissue thinned, this apparent g value extrapolated toward the expected g value for a single-scattering Henyey–Greenstein function. These reports cited values of g greater than 0.90 for visible wavelengths (see figure 8). This method offers an approach toward direct measurement of $p(\theta)$ by goniometry using thicker samples.

Figure 8 plots literature data on anisotropy versus wavelength. There is a lot of variation in the data, but in general the values of g are rather high. There appears to be a trend toward increasing g as the wavelength increases. This observation, if true, is surprising. If the small

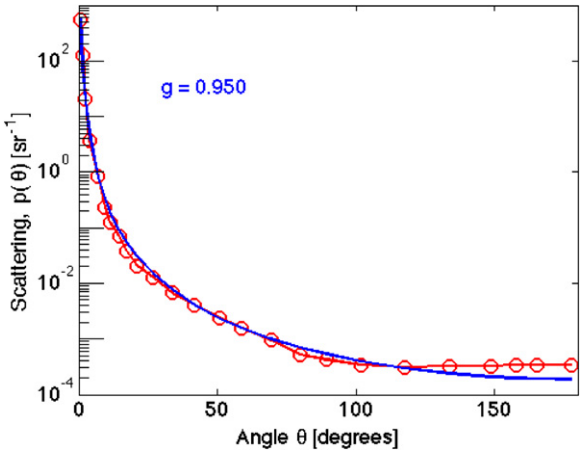

Figure 7. Angular scattering function, $p(\theta)$ (sr^{-1}), of cells at 633 nm wavelength. Data from Xu *et al* (2008). The blue line is a Henyey–Greenstein fit to the data. The $p(\theta)$ function has been properly normalized to satisfy equation (6).

sub-wavelength structures within a cell are scattering light, then as the wavelength increases the ratio of structure size to wavelength should decrease, and the scattering should become more Rayleigh-like, i.e. lower g. Why does g increase with increasing λ? This contradiction between experiment and expectation is an opportunity to better understand the nature of light scattering in tissues. Perhaps the Mie scattering from the nuclei dominates in certain experiments, which keeps g high. Perhaps there is some mesoscopic scale of structure in tissue, $\gg 10$ μm, that generates constructive interference so that more light is forward-scattered and hence g increases. The efficiency of the smallest scatterers decreases as λ increase, and perhaps their contribution to the apparent g simply diminishes, yielding a higher g at longer wavelengths. Because of the importance of g in microscopy and interferometry, more studies on anisotropy should be a priority.

4. The refractive index, *n*

The complex refractive index, $n = n' + jn''$, includes the real refractive index, n', which describes energy storage and hence affects the speed of light in a medium. The imaginary refractive index, n'', describes energy dissipation and specifies the absorption coefficient, $\mu_a = 4\pi n''/\lambda$. To a first approximation, the value of n' scales as the water content (W) of a tissue.

$$n' = n'_{\text{dry}} - (n'_{\text{dry}} - n'_{\text{water}})W, \tag{3}$$

where n'_{dry} is the refractive index of the tissue's dry mass and n'_{water} is the refractive index of water. Jacques and Prahl (1987) estimated that $n'_{\text{water}} = 1.33$ and $n'_{\text{dry}} = 1.50$, based on an old Bausch and Lomb graphic that had plotted n' versus water content for various biological materials and food products. A more recent report by Biswas and Luu (2011) on a range of biological tissues used magnetic resonance imaging (MRI) to indicate that $\rho_{\text{dry}} = 1.53$ g cm^{-3} and $n'_{\text{dry}} = 1.514$. Figure 9 summarizes their data illustrating this relationship.

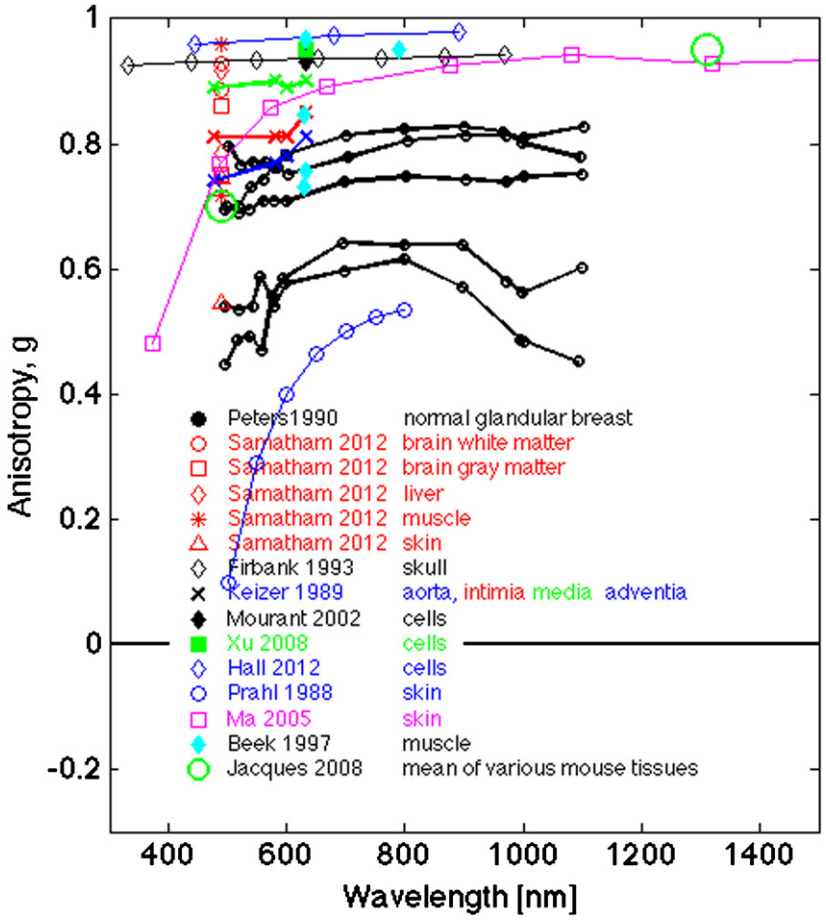

Figure 8. The anisotropy of scattering versus wavelength.

5. Absorption coefficient μ_a

A light-absorbing medium will absorb a fraction of incident light per incremental pathlength of travel within the medium. The absorption coefficient μ_a (cm^{-1}) is defined as

$$\mu_a = -\frac{1}{T}\frac{\partial T}{\partial L}, \tag{4}$$

where T (dimensionless) is the transmitted or surviving fraction of the incident light after an incremental pathlength ∂L (cm). This fractional change $\partial T/T$ per ∂L yields an exponential decrease in the intensity of the light as a function of increasing pathlength L:

$$T = \mathrm{e}^{-\mu_a L} = 10^{-\varepsilon CL} = \mathrm{e}^{-4\pi n'' L/\lambda}. \tag{5}$$

Equation (5) also cites two alternative expressions using alternative descriptors for absorption. The first spectrometers measured the transmission through a nonscattering medium containing a chromophore as $T = 10^{-\varepsilon CL}$, where C is the concentration ((mol L^{-1}) or (M)) and ε is the extinction coefficient (cm^{-1} M^{-1}) for the chromophore. Historically, ε has been recorded in the literature using this base 10 nomenclature. Optical wave theory describes

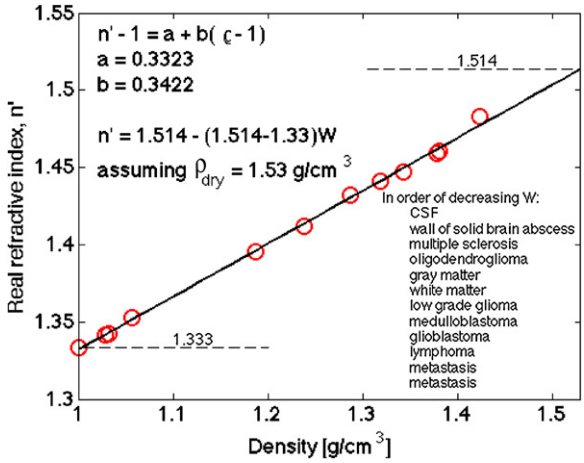

Figure 9. The real refractive indexof biological tissues, measured with an Abbé refractometer, versus the density (g cm^{-3}) (data from table in Biswas and Luu (2011)). The authors used MRI to determine the water content (W), which suggested the dry mass density was $\rho_{dry} = 1.53$ g cm^{-3}. Using this value, the relationship n' versus W can be specified, as in equation (3).

transmission of intensity as $T = \exp(-4\pi n''L/\lambda)$, where n'' is the imaginary refractive index of the medium, hence $\mu_a = 4\pi n''/\lambda$. You can find the absorption of a chromophore recorded in these three different ways, ε, μ_a and n'', but they are equivalent descriptors.

The absorption coefficient μ_a of a tissue is the sum of contributions from all absorbing chromophores within the tissue:

$$\mu_a = \ln(10) \sum_i C_i \varepsilon_i. \tag{6}$$

For example, consider HGb. The HGb mass concentration within blood, $C_{m.HGb}$ (g L^{-1}), varies for men (138 to 172 g L^{-1}), women (121 to 151 g L^{-1}), children (110 to 160 g L^{-1}) and pregnant women (110 to 120 g L^{-1}) (Tresca 2012). But the blood volume fraction (B) in a tissue also varies. The molecular weight of HGb is MW = 64 458 g mol^{-1} (van Beekvelt *et al* 2001). If $B = 0.01$ and $C_{m.HGb} = 150$ g L^{-1}, then the apparent average HGb molar concentration in the tissue is $C_{HGb} = BC_{m.HGb}/MW = (0.01)(150\ g\ L^{-1})/(64\,458\ g\ mol^{-1}) = 2.33 \times 10^{-5}$ M. The extinction coefficient of HGb varies with its oxygen saturation and with wavelength. At the isobestic point at ~806 nm, both oxyHGb and deoxyHGB have the same absorption, and the value of ε is ~818 cm^{-1} M^{-1}. At 806 nm, the contribution of blood ($B = 0.01$) to the tissue absorption is $\mu_a = \ln(10)C_{HGb}\varepsilon = (2.302)(2.33 \times 10^{-5}\ M)(818) = 0.0438\ cm^{-1}$.

Sometimes one wishes to describe the absorption properties of a material that does not have a well defined concentration, and an alternative concentration must be used, for example, C (mg mL^{-1}), and an alternative extinction coefficient must be used, ε (cm^{-1} (mg $mL^{-1})^{-1}$). The product εC still has units of cm^{-1}, and εCL is dimensionless. So, while the literature usually uses C (M), ε (cm^{-1} M^{-1}) and L (cm), alternative units for C, ε and L may be used, as long as εCL is dimensionless.

Studies on tissue optical properties will usually cite values of a tissue's average absorption coefficient μ_a, since the molecular composition of the tissue is not well specified. It is convenient to modify equation (6) so that the equation uses the volume fraction of a tissue

component ($f_{v.i}$ (L L^{-1}) or (dimensionless)) and the absorption coefficient of that pure component ($\mu_{a.i}$ (cm^{-1})). Using this approach, equation (6) can be rewritten as

$$\mu_a = \sum_i f_{v.i}\mu_{a.i}. \tag{7}$$

For example, sometimes it is helpful to describe the apparent blood volume fraction B in a tissue rather than citing an average C_{HGb} in the tissue. Citing B conveys a more anatomical sense of the density of vasculature. If one adopts the convention followed by Prahl (2012a) of assigning whole blood the HGb mass concentration $C_{\mathrm{m.HGb}} = 150$ g L^{-1}, then in equation (7) the $f_{v.\mathrm{blood}}$ would equal B. The $\mu_{a.\mathrm{blood}}$ would equal $\varepsilon_{\mathrm{blood}}\ln(10)C_{\mathrm{m.HGb}}/\mathrm{MW} = \varepsilon_{\mathrm{blood}}\ln(10)$ (150 g L^{-1})/(64 458 g mol^{-1}) $= 0.0536\varepsilon_{\mathrm{blood}}$, where $\varepsilon_{\mathrm{blood}}$ varies with wavelength. At the isobestic point $\varepsilon_{\mathrm{blood}} = 818$ cm^{-1}, as above, and the value of $\mu_{a.\mathrm{blood}}$ becomes 4.38 cm^{-1}. If a tissue has an average volume fraction ($f_{v.\mathrm{blood}} = B = 0.01$) of blood, then the blood contribution to μ_a equals (0.01)(4.38 cm^{-1}) = 0.0438 cm^{-1}.

Another example is water content. The imaginary refractive index of water at 970 nm is $n'' = 3.47 \times 10^{-6}$. The absorption coefficient of water at $\lambda = 970$ nm is $\mu_{a.\mathrm{water}} = 4\pi n''/\lambda =$ 0.45 cm^{-1}. If a tissue has a volume fraction of water $f_{v.\mathrm{water}} = 0.65$, then the contribution of water to the total tissue absorption at 970 nm is $\mu_a = f_{v.\mathrm{water}}\mu_{a.\mathrm{water}} = (0.65)(0.45\ cm^{-1}) =$ 0.29 cm^{-1}.

There are a variety of chromophores, both natural and exogenously supplied, which can contribute to μ_a in equation (6) or (7). Usually, blood and water will dominate the absorption. Sometimes, melanin, fat, bilirubin, beta-carotene or an additive such as indocyanine green must be considered. Other chromophores offer quite minor contributions. If one is interested in spectroscopic detection, then the minor contributions are important. If one is interested in understanding light penetration into a tissue for some therapeutic protocol, then the minor contributions usually do not significantly perturb the light transport.

5.1. Blood

The absorption coefficient of whole blood is shown in figure 10, using data compiled by Prahl (2012a), citing data from Gratzer and Kollias (1999), Moaveni (1970), Schmitt (1986) Takatani and Graham (1987). Figure 10(a) shows fully oxygenated blood, and figure 10(b) shows fully deoxygenated blood. Reliable data beyond 1000 nm wavelength is difficult to find in the literature. In figure 10, dashed red lines extrapolate data beyond 1000 nm, either using a Gaussian or an exponential, indicating where water absorption might begin to dominate over HGb absorption.

5.2. Water

The water absorption spectrum is plotted in figure 11(a), based on the work of Hale and Querry (1973), Zolotarev *et al* (1969) and Segelstein (1981), as cited on the website by Prahl (2012b). Figure 11(b) shows the difference between free water and bound water reported by Chung *et al* (2012), in which the absorption of bound water slightly sharpens the absorption peak at about 970 nm, i.e., absorption of bound water decreases above and below 970 nm relative to free water.

If interested in water absorption during exposure to high energy laser pulses, the report of Cummings and Walsh (1993) discusses how the mid-infrared water absorption near 3 μm wavelength broadens and the peak absorption decreases as the pulsed laser energy deposition (J cm^{-3}) in the water increases.

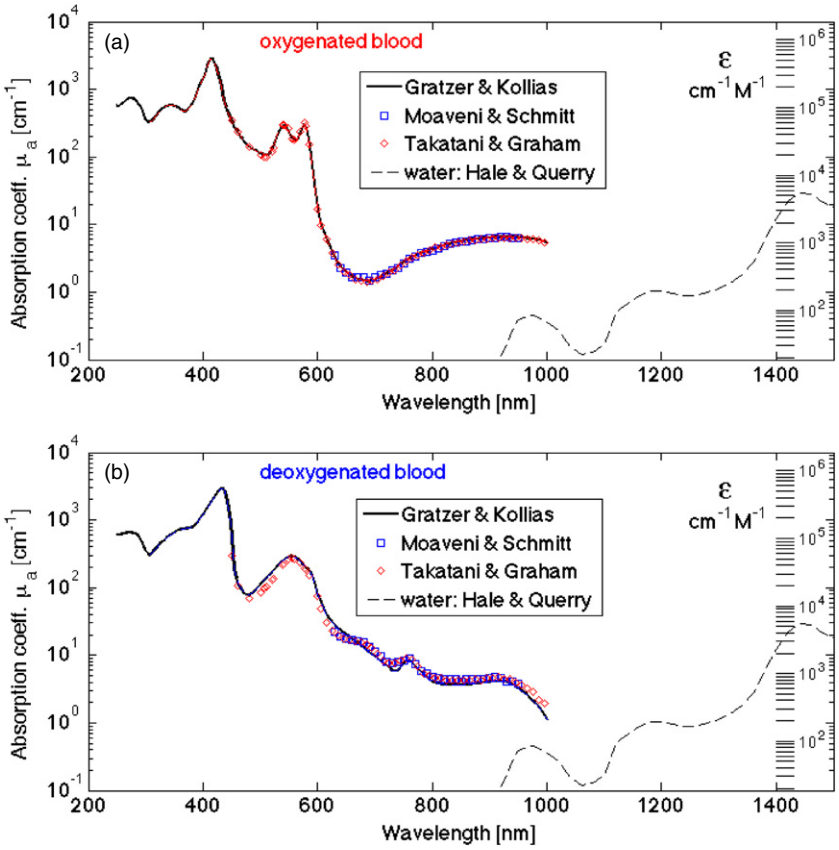

Figure 10. Absorption coefficient of whole blood versus wavelength. (Data from Prahl (2012a), citing data from Gratzer and Kollias (1999), Moaveni (1970), Schmitt (1986), Takatani and Graham (1987).) Dashed red lines extrapolate data beyond 1000 nm, either using a Gaussian or an exponential, indicating where water absorption might begin to dominate over HGb absorption. (a) Oxygenated whole blood. (b) Deoxygenated whole blood.

5.3. Melanin

The absorption coefficient of the interior of a typical cutaneous melanosome, $\mu_{a.\text{melanosome}}$ (cm^{-1}), is shown in figure 12 (open black symbols), based on the work of Jacques and McAuliffe (1991). In that report, the threshold radiant exposure, H (J cm^{-3}), of a ruby laser (690 nm wavelength) for causing explosive vaporization of melanosomes within cadaver skin was tested as a function of initial tissue temperature. A colder initial temperature required a higher laser pulse energy to pop the melanosomes. The results predicted the threshold temperature for explosive vaporization to be 112 °C. This value was used to interpret the literature of reported values of threshold H for exploding cutaneous melanosomes using a variety of lasers at various wavelengths. The analysis yielded the μ_a for the interior of cutaneous melanosomes. The resulting spectrum was consistent with optical fiber spectra for the ventral versus sun-exposed dorsal forearm skin of subjects; the difference in optical density attributed to cutaneous melanin (red circles, scaled to match laser results). The figure also shows the optical fiber probe measurements of Zonios *et al* (2008), again scaled to match laser results. The data of Sarna and Swartz (1988) specified the extinction coefficient

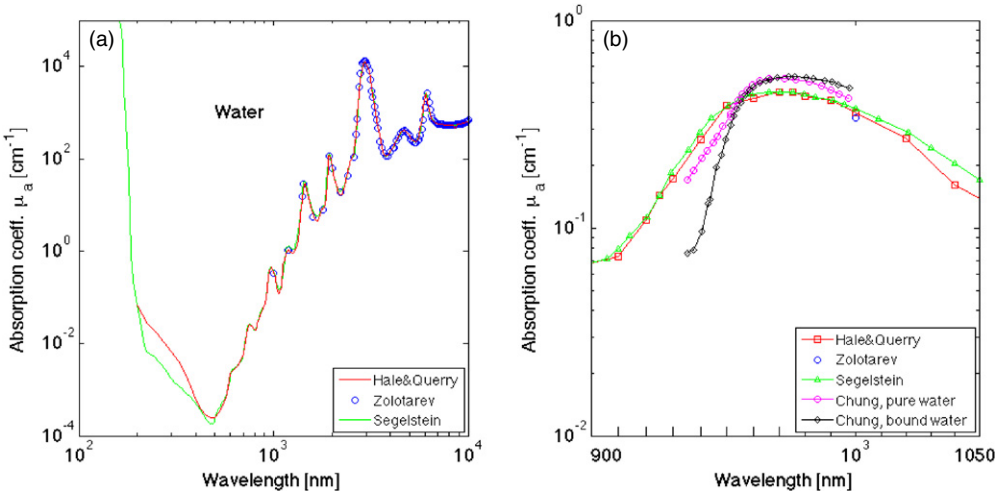

Figure 11. Absorption coefficient of water versus wavelength. (a) Data from Hale and Querry (1973), Zolotarev *et al* (1969) and Segelstein (1981). (b) Data on free versus bound water from Chung *et al* (2012), showing the drop in absorption above and below the peak at about 970 nm for bound water.

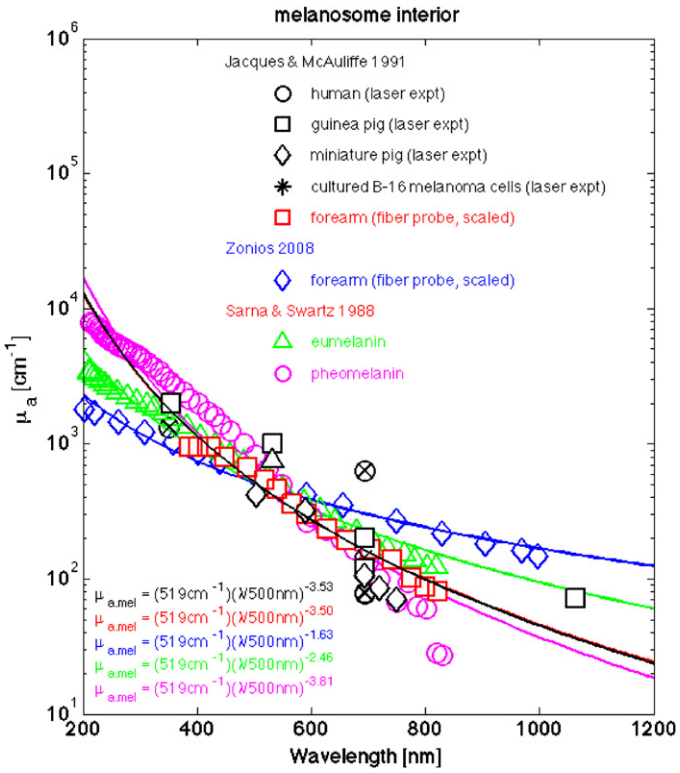

Figure 12. Absorption coefficient of the interior of a typical cutaneous melanosome versus wavelength, $\mu_{a,\text{melanosome}}$ (cm^{-1}).

ε ($\mathrm{cm^{-1}\,M^{-1}}$) of monomers for eumelanin and pheomelanin. In figure 11, these data are scaled by an intra-melanosome concentration of 461 mM for eumelanin monomers and 564 mM for pheomelanin monomers, in order to match the $\mu_{a.\mathrm{melanosome}}$ spectra at 500 nm. The fits use a power curve,

$$\mu_{a.\mathrm{melanosome}} = \left(519\ \mathrm{cm^{-1}}\right)\left(\frac{\lambda}{500\ \mathrm{nm}}\right)^{-m}, \tag{8}$$

where the value 519 $\mathrm{cm^{-1}}$ at 500 nm was specified by the laser experiments. The value of the power factor m cited by different reports varies as shown in the figure, and an approximate value for m is 3. More work on the absorption spectrum of *in vivo* melanin is needed.

To calculate the μ_a contribution for melanin in a tissue, one estimates the equivalent volume fraction ($f_{v.\mathrm{melanosome}}$) of cutaneous-like melanosomes within a tissue, $f_{v.\mathrm{melanin}}$, which is then multiplied by this $\mu_{a.\mathrm{melanosome}}$ to yield the contribution to the total μ_a of a tissue:

$$\mu_a \text{ due to melanin} = f_{v.\mathrm{melanosome}}\mu_{a.\mathrm{melanosome}}. \tag{9}$$

Using $f_{v.\mathrm{melanosome}}$ as a concentration of melanin may seem odd, but melanin is an extended polymer that does not have a unique molecular weight. Also, histology can document the number density of melanosomes in a tissue, so using $f_{v.\mathrm{melanosome}}$ is perhaps a more familiar metric to some people, such as pathologists. However, melanosomes do not all have the same melanin content. The $\mu_{a.\mathrm{melanosome}}$ of figure 12 is for a *typical cutaneous melanosome*, predominantly eumelanin, used as a convention. The figure shows the difference between eumelanin (black) and pheomelanin (red).

Alternatively, one can cite the apparent concentration of monomers ($C_{\mathrm{eumelanin}}$ and $C_{\mathrm{pheomelanin}}$ (M)) in a tissue and use the extinction coefficients of Sarna and Swartz (1988),

$$\begin{aligned}\varepsilon_{\mathrm{eumelanin}} &= \left(2.37\times10^{4}\ \mathrm{cm^{-1}\,M^{-1}}\right)\mathrm{e}^{-0.0056\lambda},\\ \varepsilon_{\mathrm{pheomelanin}} &= \left(1.01\times10^{5}\ \mathrm{cm^{-1}\,M^{-1}}\right)\mathrm{e}^{-0.0087\lambda},\end{aligned} \tag{10}$$

such that the absorption due to melanin is

$$\mu_a \text{ due to melanin} = \left(\varepsilon_{\mathrm{eumelanin}}C_{\mathrm{eumelanin}} + \varepsilon_{\mathrm{pheomelanin}}C_{\mathrm{pheomelanin}}\right)\ln(10). \tag{11}$$

5.4. Adipose tissue and fat

The absorption coefficient spectra of several fatty tissues are shown in figure 13. The work of van Veen *et al* (2004) involved careful purification and dehydration of porcine fat before measurement, and perhaps is the best spectra available at this point. Other measurements are on tissues of unknown fat and water content. An attempt to correct for the fat and water content has been made, and the spectra are in general agreement that the dominant absorption peak is at 930 nm.

5.5. Yellow pigments

The yellow pigments, bilirubin and β-carotene, are sometimes present to a small degree in the absorption spectra of tissues. Bilirubin absorption in the skin is routinely used to detect hyperbilirubinemia in neonates. β-carotene can also give a yellow hue to tissues. Figure 14 cites the extinction coefficient for bilirubin and β-carotene. Dr Angelo Lamola provided the spectrum of bilirubin associated with albumin in human serum (bilirubin/HSA) (Lamola 2011). A report of bilirubin in chloroform is also shown (Du *et al* 1998), illustrating the solvent effect on absorption. The β-carotene spectrum in a solvent, hexane, is shown (Du *et al* 1998) and the *in vivo* value is expected to differ slightly.

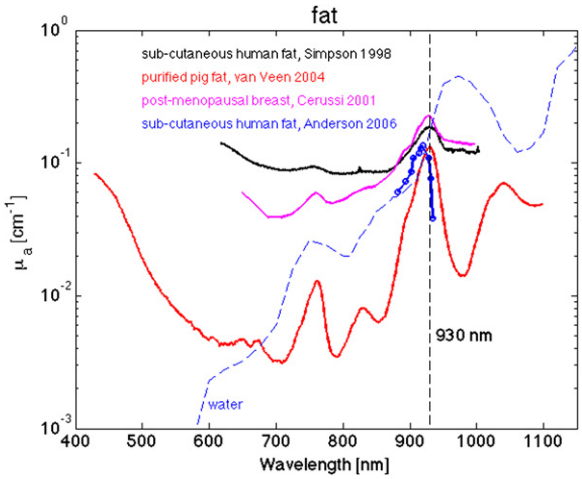

Figure 13. Absorption coefficient of fatty tissues versus wavelength. The pig fat spectrum of van Veen *et al* (2004) was highly purified. The other spectra have been corrected for fat content and corrected for the absorption by water, but the corrections are not perfect.

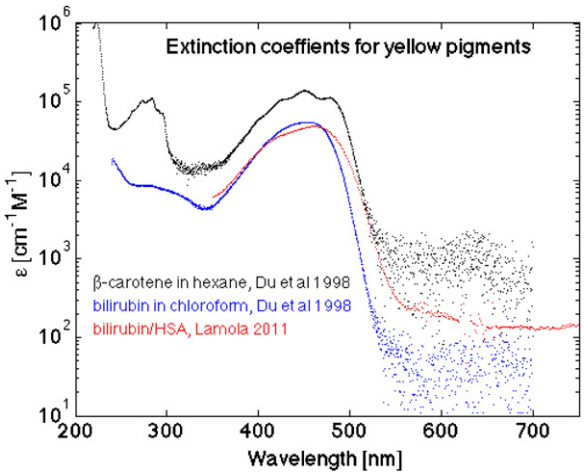

Figure 14. The extinction coefficient of bilirubin (in chloroform or bound to human serum albumin) and β-carotene (in hexane) (Du *et al* 1998, Lamola 2011).

6. A generic tissue

The optical properties of tissues should be regarded as variable from tissue to tissue, person to person and even time to time. Methods for measuring optical properties continue to improve and it is feasible to make rapid assessment of a particular tissue, much like taking a temperature with a thermometer.

For the reader who wishes to estimate optical properties to guide device or protocol design, a generic tissue can be constructed that is specified by the absorbing chromophores in the tissue and by the balance of Rayleigh and Mie scattering in the tissue.

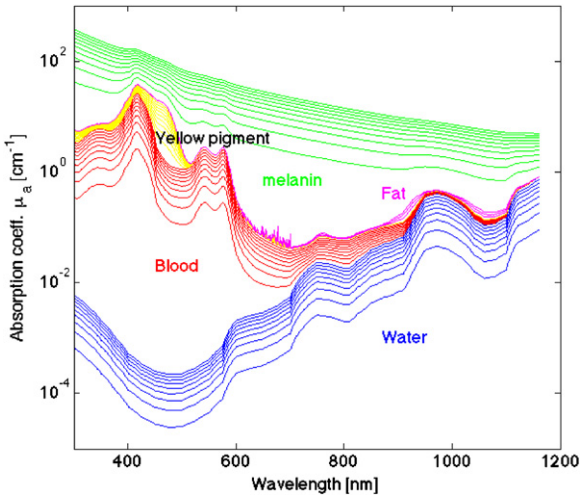

Figure 15. Total absorption coefficient μ_a (cm^{-1}), as water is added (volume fraction $f_{v.\text{water}} = 0.1$ by 0.1 to 0.9), blood at 75 oxygen saturation is added (average $f_{v.\text{blood}} = 10^{-4}$ by 10^{-4} to 2×10^{-3}), bilirubin is added (1 by 1 to 20 mg dL^{-1}, where 20 mg dL^{-1} = 342 μM is a bilirubin concentration in the blood of a jaundiced neonate), fat is added ($f_{v.\text{fat}} = 0.3$ by 0.3 to 0.9), and melanin is added ($f_{v.\text{melanosome}} = 0.01$ by 0.01 to 0.10).

Figure 15 shows the absorption coefficient μ_a increasing as water, blood, bilirubin, fat and melanin are sequentially added. This figure does not describe a real tissue, but simply illustrates the spectral consequence of the various absorbing chromophores. Any tissue can be characterized by

S	HGb oxygen saturation of mixed arterio-venous vasculature
B	average blood volume fraction ($f_{v.\text{blood}}$)
W	water content ($f_{v.\text{water}}$)
Bili	bilirubin concentration (C (M))
βC	β-carotene concentration (C (M))
F	fat content ($f_{v.\text{fat}}$)
M	melanosome volume fraction ($f_{v.\text{melanosome}}$), or alternatively the molar concentration of melanin monomers (C (M)).

The total absorption coefficient is calculated

$$\mu_a = BS\mu_{a.\text{oxy}} + B(1-S)\mu_{a.\text{deoxy}} + W\mu_{a.\text{water}} + F\mu_{a.\text{fat}} + M\mu_{a.\text{melanosome}} + 2.3C_{\text{bili}}\varepsilon_{\text{bili}} + 2.3C_{\beta\text{C}}\varepsilon_{\beta\text{C}}. \quad (12)$$

Figure 16 shows a more realistic tissue, in which the blood content is fixed at $B = 0.002$, $S = 0.75$, and there is a baseline volume fraction of fibrous material, $f_{v.\text{fibrous}} = 0.30$. The tissue fat content and water content offset each other, with $F = [0$ by 0.1 to $0.7]$ as $W = [0.7$ by -0.1 to $0.1]$ such that fat + water = 0.70. The fat signature is evident at water contents below 30, but is less obvious at higher water contents.

Figure 17 shows the generic reduced scattering coefficient of tissues, based on equation (2). The contribution of Mie scattering (a_{Mie}) is shown as blue lines. The contribution of Rayleigh scattering (a_{Rayleigh}) is added to the highest Mie scattering, and the combination is shown as red lines ($a_{\text{Rayleigh}} + a_{\text{Mie}}$). As the Rayleigh component of scattering increases, the short wavelength scattering increases significantly.

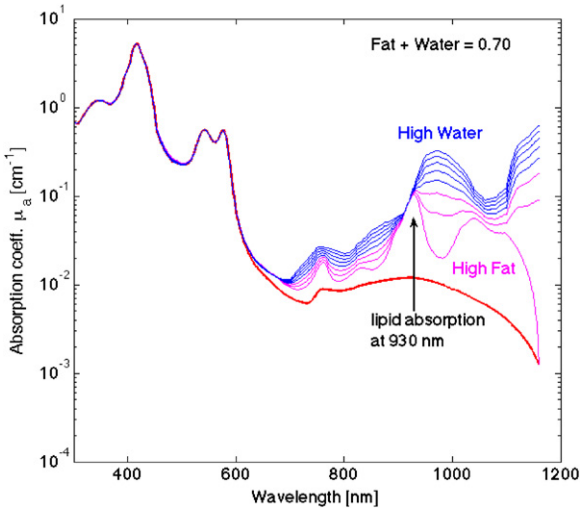

Figure 16. The absorption spectrum of a tissue ($B = 0.002$, $S = 0.75$, $f_{v.\text{fibrous}} = 0.30$) that varies its water content from 0 by 0.1 to 0.7 as the fat content varies from 0.7 by 0.1 to 0, such that fat + water = 0.7. Magenta lines are for high fat, low water, and the fat signature is clearly present at 930 nm (arrow). The blue lines are for low fat, high water ($W \geqslant 0.3$), and the fat signature is less obvious. (Based on the fat spectrum of van Veen *et al* (2004).)

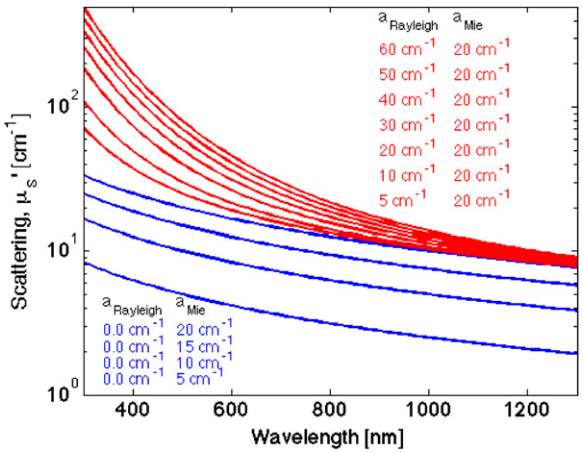

Figure 17. Generic scattering. The reduced scattering coefficient, μ_s' (cm^{-1}), of a generic tissue, with variable contributions from Rayleigh and Mie scattering. The contribution of Mie scattering is shown as blue lines ($a_{\text{Mie}} = 5$ to 20 cm^{-1}, $a_{\text{Rayleigh}} = 0$). The Rayleigh scattering ($a_{\text{Rayleigh}} = 5$ to 60 cm^{-1}, $a_{\text{Mie}} = 20$ cm^{-1}) plus Mie scattering is shown as red lines ($a_{\text{Rayleigh}} + a_{\text{Mie}}$).

Equations (1), (2) and (6), (7) can mimic the optical properties of a generic tissue at any wavelength, but one must specify the tissue parameters in these equations. The literature is limited in its reporting of *in vivo* optical properties. The task now is to better understand the constitution of tissues in terms of tissue chromophores and tissue parameters that govern absorption to enable use of the generic model. Table 3 lists a brief survey of the *in vivo* optical parameters that affect absorption (C_{HGb}, B, S, W, M, F).

Table 3. *In vivo* tissue parametersgoverning optical absorption. C_{HGb} = total HGb concentration (μM), B = blood volume fraction × 100% (assuming 150 g HGb L^{-1} blood), S = oxygen saturation of HGb × 100%, W = water volume fraction × 100%, M = melanosome volume fraction × 100%. Human tissues unless otherwise labeled. (na = not available.)

Tissue (reference)	C_{HGb} (μM)	B%	S%	W%	F%	M%
1 Breast, normal (Tromberg *et al* 1997)	23.6	1.02	67.6	14.4	65.6	0
2 Breast, normal (Bevilacqua *et al* 2000)	24.2	1.04	75.5	29.2	51.7	0
3 Breast, normal (Durduran *et al* 2002)	34.0	1.46	68.0	na	na	0
4 Breast, normal (Jakubowski *et al* 2004)	16.0	0.69	62.6	6.0	74.0	0
5 Breast, normal (Spinelli *et al* 2004)	15.7	0.67	66.4	14.5	58.0	0
6 Breast, tumor (Jakubowski *et al* 2004)	41.0	1.76	61.1	41.0	39.0	0
7 Abdomen (Jakubowski *et al* 2004)	12.5	0.54	76.0	11.0	69.0	0
8 Dermis (Choudhury *et al* 2010)	4.7	0.20	39.0	65.0	0	0
9 Epidermis (Choudhury *et al* 2010)	0	0	0	na	na	2.50
10 Skin I–II (500–600 nm) (Tseng *et al* 2011)	1.1	0.05	75.7	na	na	1.65
11 Skin I–II (600–1000 nm) (Tseng *et al* 2011)	7.9	0.34	98.5	21.4	27.7	0.87
12 Skin III–IV (500–600 nm) (Tseng *et al* 2011)	8.2	0.35	96.2	na	na	1.98
13 Skin III–IV (600–1000 nm) (Tseng *et al* 2011)	9.6	0.41	99.2	26.1	22.5	1.15
14 Skin V–VI (600–1000 nm) (Tseng *et al* 2011)	2.7	0.12	99.3	16.6	18.7	1.65
15 Forearm (Matcher *et al* 1997)	117.0	5.03	64.1	na	na	na
16 Head (Matcher *et al* 1997)	78.0	3.35	64.1	na	na	na
17 Calf (Matcher *et al* 1997)	84.0	3.61	69.0	na	na	na
18 Neonatal brain (Zhao *et al* 2004)	39.7	1.71	58.7	na	na	0
19 Neonatal brain (Ijichi *et al* 2005)	64.7	2.78	70.0	na	na	0
20 Prostate (Svensson 2007)	215.0	9.24	76.0	na	na	0
21 Canine bowel (Solonenko *et al* 2002)	119.0	5.11	80.0	na	na	0
22 Canine kidney (Solonenko *et al* 2002)	340.0	14.61	70.0	na	na	0
23 Canine prostate (Solonenko *et al* 2002)	51.0	2.19	50.0	na	na	0
24 Canine myocardium (Eliasen *et al* 1982)	100.1	4.30	na	na	na	0
25 Rat brain cortex (Todd *et al* 1992)	58.2	2.50	na	na	na	0
26 Rat brain cortex (Abookasis *et al* 2009)	87.3	3.75	60.7	na	na	0
27 Rat brain cortex normal (O'Sullivan *et al* 2012)	71.0	3.05	59.0	na	na	0
28 Rat brain cortex occluded (O'Sullivan *et al* 2012)	65.0	2.79	na	na	na	0
29 Sheep&horse brain (Weaver *et al* 1989)	32.9	1.42	na	na	na	0
30 Sheep&horse heart (Weaver *et al* 1989)	160.6	6.90	na	na	na	0
31 Sheep&horse lung (Weaver *et al* 1989)	1355.5	58.25	na	na	na	0
32 Sheep&horse liver (Weaver *et al* 1989)	1151.9	49.50	na	na	na	0
33 Sheep&horse kidney (Weaver *et al* 1989)	723.7	31.10	na	na	na	0
34 Sheep&horse small intestine (Weaver *et al* 1989)	214.1	9.20	na	na	na	0
35 Sheep&horse large intestine (Weaver *et al* 1989)	151.3	6.50	na	na	na	0
36 Sheep&horse muscle (Weaver *et al* 1989)	27.0	1.16	na	na	na	0
37 Sheep&horse tongue (Weaver *et al* 1989)	216.4	9.30	na	na	na	0
38 Sheep&horse skin (Weaver *et al* 1989)	36.4	1.57	na	na	na	0
39 Sheep&horse subcut. fat (Weaver *et al* 1989)	17.7	0.76	na	na	na	0
40 Sheep&horse omental fat (Weaver *et al* 1989)	60.7	2.61	na	na	na	0
41 Sheep&horse cortical bone (Weaver *et al* 1989)	31.6	1.36	na	na	na	0
42 Sheep&horse rib bone (Weaver *et al* 1989)	69.8	3.00	na	na	na	0
43 Sheep&horse adrenal (Weaver *et al* 1989)	274.6	11.80	na	na	na	0
44 Sheep&horse pancreas (Weaver *et al* 1989)	300.2	12.90	na	na	na	0
45 Sheep&horse ovary (Weaver *et al* 1989)	74.0	3.18	na	na	na	0
46 Sheep&horse uterus (Weaver *et al* 1989)	131.5	5.65	na	na	na	0
47 Sheep&horse mammary (Weaver *et al* 1989)	1.0	0.04	na	na	na	0

The data in table 3 lists average tissue parameters that affect scattering (a, b, a', f_{Ray}, b_{Mie}). Many of these data were measured on excised tissues. The optical scattering properties of excised tissues are relatively stable for a short time (hours) if one avoids overhydration

by soaking in saline or dessication by exposure to ambient air, and the data of table 2 are representative of *in vivo* optical scattering properties. But there is one distinct exception. The optical scattering of white matter of the brain drastically decreases upon excision, on the order of minutes.

Certainly, more work on *in vivo* tissue measurements is needed, reporting both tissue optical properties and tissue parameters as in tables 1–3.

7. Conclusion

The use of a generic tissue can adequately mimic any real tissue, and has the advantage of generating smoothly predictable spectra for absorption and scattering. The generic equations, equations (1) or (2) for scattering and equations (6) or (7) for absorption allow calculation of the expected optical properties versus wavelength of tissues with varying chromophore content and ultrastructural character. The average tissue parameters (C_{HGb} or B, S, W, M, F, and a, b or a', f_{Ray}, b_{mie}) can specify the wavelength dependence of tissue optical properties and guide design of devices, diagnostics and treatment protocols. However, the variation from subject to subject, site to site and time to time argues for real-time optical property measurements on patients when working with individuals.

References

Abookasis D, Lay C C, Mathews M S, Linskey M E, Frostig R D and Tromberg B J 2009 Imaging cortical absorption, scattering, and hemodynamic response during ischemic stroke using spatially modulated near-infrared illumination *J. Biomed. Opt.* **14** 024033

Alexandrakis G, Rannou F R and Chatziioannou A F 2005 Tomographic bioluminescence imaging by use of a combined optical-PET (OPET) system: a computer simulation feasibility study *Phys. Med. Biol.* **50** 4225–41

Anderson R R and Parrish J A 1982 Optical properties of human skin in *The Science of Photomedicine* ed J D Regan and J A Parrish (New York: Plenum Press) chapter 6, pp 147–94

Anderson R R *et al* 2006 Selective photothermolysis of lipid-rich tissues: A free electron laser study *Laser Surg. Med.* **38** 913–19

Bashkatov A N, Genina E A and Tuchin V V 2011 Optical properties of skin, subcutaneous, and muscle tissues: a review *J. Innovative Opt. Health Sci.* **4** 9–38

Beauvoit B, Evans S M, Jenkins T W, Miller E E and Chance B 1995 Correlation between the light scattering and the mitochondrial content of normal tissues and transplantable rodent tumors *Anal. Biochem.* **226** 167–74

Beek J P, van Staveren H J, Posthumus P, Sterenborg H J C M and van Gemert M J C 1997 The optical properties of lung as a function of respiration *Phys. Med. Biol.* **42** 2263–72

Bevilacqua F, Berger A J, Cerussi A E, Jakubowski D and Tromberg B J 2000 Broadband absorption spectroscopy in turbid media by combined frequency-domain and steady-state methods *Appl. Opt.* **39** 6498–507

Bevilacqua F, Piguet D, Marquet P, Gross J D, Tromberg B J and Depeursinge C 1999 *In vivo* local determination of tissue optical properties: applications to human brain *Appl. Opt.* **38** 4939–50

Biswas T K and Luu T M 2011 *In vivo* MR measurement of refractive index, relative water content and T2 relaxation time of various brain lesions with clinical application to discriminate brain lesions *Internet. J. Radiol.* **13** No 1

Cerussi A E, Berger A J, Bevilacqua F, Shah N, Jakubowski D, Butler J, Holcombe R F and Tromberg B J 2001 Sources of absorption and scattering contrast for near-infrared optical mammography *Acad. Radiol.* **8** 211–8

Cheong W F 1995 Appendix to chapter 8: Summary of optical properties *Optical-Thermal Response of Laser-Irradiated Tissue* 1st edn ed A J Welch and M J C van Gemert (New York: Plenum)

Choudhury N, Samatham R and Jacques S L 2010 Linking visual appearance of skin to the underlying optical properties using multi-spectral imaging *Proc. SPIE* **7548** 75480G-1

Chung S H, Yu H, Su M-Y, Cerussi A E and Tromberg B J 2012 Molecular imaging of water binding state and diffusion in breast cancer using diffuse optical spectroscopy and diffusion weighted MRI *J. Biomed. Opt.* **17** 071304

Cummings J P and Walsh J T 1993 Erbium laser ablation: the effect of dynamic optical properties *Appl. Phys. Lett.* **62** 1988–90

Du H, Fuh R A, Li J, Corkan A and Lindsey J S 1998 PhotochemCAD: a computer-aided design and research tool in photochemistry *Photochem. Photobiol.* **68** 141–2

Durduran T, Choe R, Culver J P, Zubkov L, Holboke M J, Giammarco J, Chance B and Yodh A G 2002 Bulk optical properties of healthy female breast tissue *Phys. Med. Biol.* **47** 2847–61

Eliasen P, Amtorp O, Tøndevold E and Haunsø S 1982 Regional blood flow, microvascular blood content and tissue haematocrit in canine myocardium *Cardiovasc. Res.* **16** 593–8

Firbank H, Hiraoka M, Essenpreis M and Delpy D T 1993 Measurement of the optical properties of the skull in the wavelength range 650–950 nm *Phys. Med. Biol.* **38** 503–10

Gareau D S 2006 *In vivo* confocal microscopy in turbid media *PhD Dissertation* Oregon Health & Science University

Gratzer W B and Kollias N 1999 Personal communication from Gratzer, Med. Res. Council Labs, Holly Hill, London, and N Kollias, Wellman Laboratories, Harvard Medical School, Boston (as compiled and posted on http://omlc.ogi.edu/spectra/hemoglobin/ by S A Prahl)

Hale G M and Querry M R 1973 Optical constants of water in the 200 nm to 200 μm wavelength region *Appl. Opt.* **12** 555–63

Hall G, Jacques S L, Eliceiri K W and Campagnola P J 2012 Goniometric measurements of thick tissue using Monte Carlo simulations to obtain the single scattering anisotropy coefficient *Biomed. Opt. Express* **3** 2707–19

Ijichi S, Kusaka T, Isobe K, Okubo K, Kawada K, Namba M, Okada H, Nishida T, Imai T and Itoh S 2005 Developmental changes of optical properties in neonates determined by near-infrared time-resolved spectroscopy *Pediatr. Res.* **58** 568–73

Jacques S L 1996 Origins of tissue optical properties in the UVA, visible and NIR regions *OSA TOPS on Advances in Optical Imaging and Photon Migration* vol 2 ed R R Alfano and J G Fujimoto (Washington DC: Optical Society of America) pp 364–71

Jacques S L, Alter C A and Prahl S A 1987 Angular dependence of HeNe laser light scattering by human dermis *Lasers Life Sci.* **1** 309–34

Jacques S L and McAuliffe D J 1991 The melanosome: threshold temperature for explosive vaporization and internal absorption coefficient during pulsed laser irradiation *Photochem. Photobiol.* **53** 769–76

Jacques S L and Pogue B W 2008 Tutorial on diffuse light transport *J. Biomed. Opt.* **13** 041302

Jacques S L and Prahl S A 1987 Modeling optical and thermal distributions in tissue during laser irradiation *Lasers in Surg. Med.* **6** 494–503

Jacques S L, Samatham R, Choudhury N, Fu Y and Levitz D 2008 Measuring tissue optical properties *in vivo* using reflectance-mode confocal microscopy and OCT *Proc. SPIE* **6864** 68640B

Jakubowski D B, Cerussi A E, Bevilacquia F, Shah N, Hsiang D, Butler J and Tromberg B J 2004 Monitoring neoadjuvant chemotherapy in breast cancer using quantitative diffuse optical spectroscopy: a case study *J. Biomed. Opt.* **9** 230–8

Keijzer M, Jacques S L, Prahl S A and Welch A J 1998 Light destributions in artery tissue: Monte Carlo simulations for finite-diameter laser beams *Laser Surg. Med.* **9** 148–54

Kim A and Wilson B C 2011 Measurement of *ex vivo* and *in vivo* tissue optical properties: methods and theories *Optical-Thermal Response of Laser-Irradiated Tissue* 2nd edn ed A J Welch and M J C van Gemert (Berlin: Springer) chapter 8, DOI:10.1007/978-90-481-8831-4

Lamola A 2011 The extinction coefficient of bilirubin associated with albumin in human serum personal communication

Ma X, Lu J Q, Ding H and Hu X-H 2005 Bulk optical parameters of porcine skin dermis at eight wavelength from 325 to 1557 nm *Opt. Lett.* **30** 412414

Matcher S J, Cope M and Delpy D T 1997 *In vivo* measurements of the wavelength dependence of tissue-scattering coefficients between 760 and 900 nm measured with time-resolved spectroscopy *Appl. Opt.* **36** 386–96

Moaveni M K 1970 A multiple scattering field theory applied to whole blood *PhD Dissertation* Department of Electrical Engineering, University of Washington

Mourant J R, Johnson T M, Carpenter S, Guerra A, Aida T and Freyer J P 2002 Polarized angular dependent spectroscopy of epithelial cells and epithelial cell nuclei to determine the size scale of scattering structures *J. Biomed. Opt.* **7** 378–87

Newman C and Jacques S L 1991 Laser penetration into prostate for various wavelengths *Lasers Surg. Med.* (Suppl 3) 75 abstract 310

O'Sullivan T D, Cerussi A E, Cuccia D J and Tromberg B J 2012 Diffuse optical imaging using spatially and temporally modulated light *J. Biomed. Opt.* **17** 071311

Parsa P, Jacques S L and Nishioka N 1989 Optical properties of the liver between 350 and 2200 nm *Appl. Opt.* **28** 2325–30

Peters V G, Wymant D R, Patterson M S and Frank G L 1990 Optical properties of normal and diseased human breast tissues in the visible and near infrared *Phys. Med. Biol.* **35** 1317–34

Prahl S A 1988 Light transport in tissue *PhD Dissertation* University of Texas at Austin, Texas

Prahl S A 2012a http://omlc.ogi.edu/spectra/hemoglobin A compendium of tissue optical properties

Prahl S A 2012b http://omlc.ogi.edu/spectra/water/ Optical absorption of water
Prahl S A and Jacques S L 2012 http://omlc.ogi.edu/software/mie/ Mie theory
Rogers J D, Capoglu I R and Backman V 2012 Nonscalar elastic light scattering from continuous random media in the Born approximation *Opt. Lett.* **34** 1891–3
Saidi I S, Jacques S L and Tittel F K 1995 Mie and Rayleigh modeling of visible-light scattering in neonatal skin *Appl. Opt.* **34** 7410–8
Salomatina E, Jiang B, Novak J and Yaroslavsky A N 2006 Optical properties of normal and cancerous human skin in the visible and near-infrared spectral range *J. Biomed. Opt.* **11** 064026
Samatham R 2012 Determination of optical scattering properties of tissues using reflectance-mode confocal microscopy *Dissertation* Oregon Health & Science University PhD
Samatham R, Jacques S L and Campagnola P 2008 Optical properties of mutant vs wildtype mouse skin measured by reflectance-mode confocal scanning laser microscopy (rCSLM) *J. Biomed. Opt.* **13** 041309
Sandell J L and Zhu T C 2011 A review of *in-vivo* optical properties of human tissues and its impact on PDT *J. Biophotonics* **4** 773–87
Sarna T and Swartz H M 1988 The physical properties of melanins *The Pigmentary System* ed J J Nordlund *et al* (Oxford: Oxford University Press) posted on (http://omlc.ogi.edu/spectra/melanin/extcoeff.html by S L Jacques)
Schmitt J M 1986 Optical measurement of blood oxygenation by implantable telemetry *Technical Report* G558-15, Stanford (as compiled and posted on http://omlc.ogi.edu/spectra/hemoglobin/ by S A Prahl)
Schmitt J M and Kumar G 1996 Turbulent nature of refractive-index variations in biological tissue *Opt. Lett.* **21** 1310–2
Segelstein D J 1981 The complex refractive index of water *MS Thesis* Department of Physics, University of Missouri-Kansas City
Simpson C R, Kohl M, Essenpreis M and Cope M 1998 Near infrared optical properties of *ex-vivo* human skin and subcutaneous tissues measured using the Monte Carlo inversion technique *Phys. Med. Biol.* **43** 2465–78 posted on the website (http://www.medphys.ucl.ac.uk/research/borg/research/NIRtopics/skin/skinoptprop.htm)
Solonenko M, Cheung R, Busch T M, Kachur A, Griffin G M, Vulcan T, Zhu T C, Wang H-W, Hagn S M and Yodh A G 2002 *In vivo* reflectance measurement of optical properties, blood oxygenation and motexafin lutetium uptake in canine large bowels, kidneys and prostates *Phys. Med. Biol.* **47** 857–73
Spinelli L, Torricelli A, Pifferi A, Taroni P, Danesini G M and Cubeddu R 2004 Bulk optical properties and tissue components in the female breast from multiwavelength time-resolved optical mammography *J. Biomed. Opt.* **9** 1137–42
Svensson T, Andersson-Engels S, Einarsdottir M and Svanberg K 2007 *In vivo* optical characterization of human prostate tissue using near-infrared time-resolved spectroscopy *J. Biomed. Opt.* **12** 014022
Takatani S and Graham M D 1987 Theoretical analysis of diffuse reflectance from a two-layer tissue model *IEEE Trans. Biomed. Eng.* **26** 656–64 as compiled and posted on (http://omlc.ogi.edu/spectra/hemoglobin/ by S A Prahl)
Todd M M, Weeks J B and Warner D S 1992 Cerebral blood flow, blood volume, and brain tissue hematocrit during isovolemic hemodilution with hetastarch in rats *Am. J. Physiol. Heart Circ. Physiol.* **263** H75–82
Tresca A 2012 About.com Guide (http://ibdcrohns.about.com/od/diagnostictesting/p/testhemo.htm 26 October 2012)
Tromberg B 1996 Beckman Laser Institute and Medical Clinic, University of California-Irvine, personal communication
Tromberg B J, Coquoz O, Fishkin J B, Pham T, Anderson E R, Butler J, Cahn M, Gross J D, Venugopalan V and Phan D 1997 Non-invasive measurements of breast tissue optical properties using frequency-domain photon migration *Phil. Trans. R. Soc.* B **352** 661–8
Tseng T-Y, Chen C-Y, Li Y-S and Sung K-B 2011 Quantification of the optical properties of two-layered turbid media by simultaneously analyzing the spectral and spatial information of steady-state diffuse reflectance spectroscopy *Biomed. Opt. Express* **2** 901–14
van Beekvelt M C P, Colier W N J M, Wevers R A and Van Engelen B G M 2001 Performance of near-infrared spectroscopy in measuring local O_2 consumption and blood flow in skeletal muscle *J. Appl. Physiol.* **90** 511–9
van Veen R L P, Sterenborg H J C M, Pifferi A, Torricelli A and Cubeddu R 2004 Determination of VIS–NIR absorption coefficients of mammalian fat, with time- and spatially resolved diffuse reflectance and transmission spectroscopy *OSA Annual BIOMED Topical Meeting* posted on (http://omlc.ogi.egu/spectra/fat/ by S A Prahl)
Weaver B M Q, Standdon G E and Pearson M R B 1989 Tissue blood content in anaesthetised sheep and horses *Comp. Biochem. Physiol.* A **94** 401–4
Welch A J and van Gemert M J C 2011 Overview of optical and thermal laser-tissue interaction and nomenclature *Optical-Thermal Response of Laser-Irradiated Tissue* 2nd edn ed A J Welch and M J C van Gemert (Berlin: Springer) chapter 1 (DOI:10.1007/978-90-481-8831-4)
Wilson J D, Cottrell W J and Foster T H 2007 Index-of-refraction-dependent subcellular light scattering observed with organelle-specific dyes *J. Biomed. Opt.* **12** 014010

Xu M and Alfano R R 2005 Fractal mechanisms of light scattering in biological tissue and cells *Opt. Lett.* **30** 3051–3

Xu M, Wu T T and Qu J Y 2008 Unified Mie and fractal scattering by cells and experimental study on application in optical characterization of cellular and subcellular structures *J. Biomed. Opt.* **13** 024015

Yi J and Backman V 2012 Imaging a full set of optical scattering properties of biological tissues by inverse spectroscopic optical coherence tomography *Opt. Lett.* **37** 4443–5

Zhao J, Ding H S, Hou L, Zhou C L and Chance B 2004 *In vivo* determination of the optical properties of infant brain using frequency-domain near-infrared spectroscopy *J. Biomed. Opt.* **10** 024028

Zolotarev V M, Mikhilov B A, Alperovich L L and Popov S I 1969 Dispersion and absorption of liquid water in the infrared and radio regions of the spectrum *Opt. Spectrosc.* **27** 430–2

Zonios G, Dimou A, Bassukas I, Galaris D, Tsolakidis A and Kaxiras E 2008 Melanin absorption spectroscopy: new method for noninvasive skin investigation and melanoma detection *J. Biomed. Opt.* **13** 014017